Proceedings of the 9ICEG
9th International Congress on Environmental Geotechnics
25-28 June, 2023 | Chania, Greece

https://doi.org/10.53243/ICEG2023-12

Monitoring seepage behavior of infiltrated rainwater and the transport of alkaline components within an embankment model constructed of steel slag-mixed soil

K. Kawai[1], S. Kataoka[2] and K. Nakashima[3]

[1]*Professor, Kindai University, Higashi-Osaka, Japan, kkawai@civileng.kindai.ac.jp*

[2]*Assistant Professor, Kobe University, Kobe, Japan, skataoka@people.kobe-u.ac.jp*

[3]*Assistant Professor, Kindai University, Higashi-Osaka, Japan, knakashima@civileng.kindai.ac.jp*

ABSTRACT

Though steel slag generated in the process of ironmaking becomes industrial waste when left as it is, calcium ions within the slag change into calcium carbonate and solidify over time when mixed with soil materials. Therefore, attempts have been made to recycle the slag as roadbed material and aggregate. If the steel slag-mixed soil can be used for constructing road embankments, it will lead to the reduction of industrial waste both in ironmaking and in earthmoving construction. On the downside, steel slag contains a lot of calcium, and rainfall infiltration to embankment constructed with steel slag-mixed soil can cause leachate of alkaline components around the embankment. In this study, model tests and rainfall infiltration simulations were conducted to investigate the behavior of infiltrated rainwater and of alkaline components. Embankment models were constructed with steel slag-mixed soil and exposed to natural weather conditions. Soil moisture and water pressure were monitored during the test and electrical prospecting was conducted. Moreover, rainfall infiltration was simulated using soil/water/air/soluble material coupled analysis code. Consequently, it was found that the rainwater infiltrated through slope surface tends to flow parallel to the slope while that the rainwater infiltrated through the crown tends to flow vetically. Rainwater that flows vertically and reaches to the bottom of embankment raises the phreatic surface and causes leachate of alkarine component. However, since these seepage and leachate behavior are dependent on rainfall intensity, numerical simulation is effective for designing embankment.

Keywords: Steel slag-mixed soil, Model test, Electrical prospecting, Rainfall infiltration simulation

1 INTRODUCTION

Since soil cuttings can contain harmful materials like naturally derived heavy metals, moving construction waste soil offsite without proper treatment is forbidden. Therefore, balancing the amount of cutting and filling soil onsite is important in designing earthmoving construction. However, it is difficult to use construction waste soil as fill without modification. When construction waste soil has low-quality characteristics, such as high-water content, high fine-grain content, slaking properties, and so on, it must be improved before used for earthworks. For this purpose, a solidification material is needed to improve low-quality soil. A solidification material like cement can improve the consistency, shear strength, and compressibility of low-quality soil. Steel slag, which costs less than cement, is another potential solidification material that has been experimentally investigated for applicability (Akinwumi, 2014; Goodarzi & Staimi, 2015; Hirai et al., 2012; Kataoka, 2017; Malasavage et al., 2012; Manso et al., 2013).

However, steel slag is a residual product generated in the process of ironmaking, and it is difficult to control its quality. Moreover, steel slag contains a lot of calcium. As most earth structures are exposed to natural weather conditions, it is concerning that chemical material leached from the earth structure due to external water head fluctuation, such as rainfall and elevation of the phreatic surface, may disperse into the surrounding environment. Methods of constructing and maintaining embankments without leaching when composed of soil containing chemically-active materials like calcium are required for the effective use of steel slag.

In this study, an embankment model test using steel slag-mixed soil was conducted, and rainfall infiltration behavior and alkaline component leachate from the embankment was monitored. Moreover, rainfall infiltration to the model embankment was simulated by soil/water/air/soluble material coupled finite element analysis code, and simulation results were compared to experimental results to understand leachate behavior theoretically.

2 EMBANKMENT MODEL CONSTRUCTED WITH STEEL SLAG-MIXED SOIL

Construction waste soil generated from an earthmoving construction site in Kobe and two kinds of steel slags (called steel slag S and N) were used for the embankment model. The soil particle density of the construction waste soil, steel slag S and N, were 2.65, 3.45 and 3.03 (g/cm^3), respectively. Construction waste soil and steel slag were mixed at a volume ratio of 2:1 and compacted for constructing the embankment model. Figure 1 shows the particle grading curves. It is known that mixing steel slag can improve grading by decreasing the fine content. Table 1 summarizes the particle density and pH of these mixed soils. Compaction curves and unconfined shear strength changes over the curing time of specimens compacted at the optimum water content are shown in Figure 2. The maximum dry densities can be seen around the optimum water content of 11 to 12 (%). From this, It is obvious that shear strength increases with curing time and that the effects of mixing steel slag on shear strength result from not only improving particle gradation, but also from the cementation of soil particles.

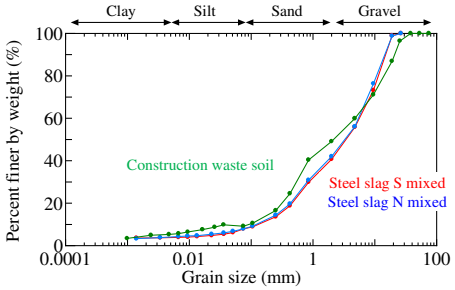

Figure 1. *Grain size accumulation curves of soil materials*

Table 1. *Properties of steel slag-mixed soils*

	Steel slag S mixed	Steel slag N mixed
Particle density	2.878(g/cm^3)	2.890(g/cm^3)
Initial pH	12.4	12.2

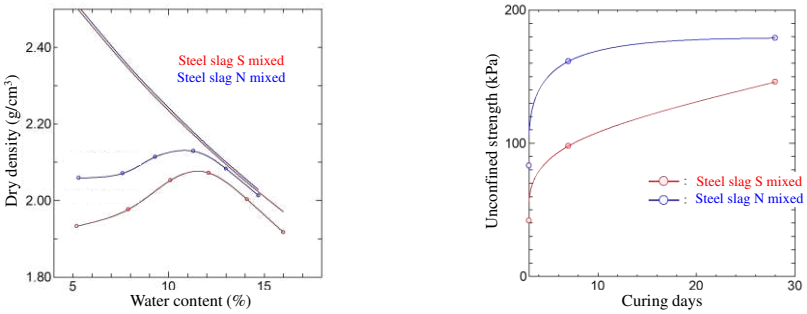

Figure 2. *Compaction curves (left) and Unconfined strength (right)*

The embankment model was constructed in September 2017. Figure 3 shows its outline. An asymmetric embankment was constructed and impermeable sheets were placed on the steeper side slope and the bottom to collect water infiltrated through the embankment at the ditch (shown in Figure 3). Each steel slag-mixed soil was compacted at 80 and 90 (%) compaction degrees for constructing the 4 kinds of embankment shown in Figure 4. Each embankment was partitioned by impermeable sheets and called S-80, S-90, N-80 and N-90, respectively. Figure 4 shows the positions of soil moisture meters and tensiometers. Circled numbers indicate channels of soil moisture meters. The measurement depths of tensiometers were 15 and 25 (cm). Moreover, electrical prospecting was conducted to identify the distribution of soil moisture within the embankment. The dipole-dipole method for alignment of

electrodes was adopted here. The pH of leachate water collected in the ditch was measured on the next day of rainfall.

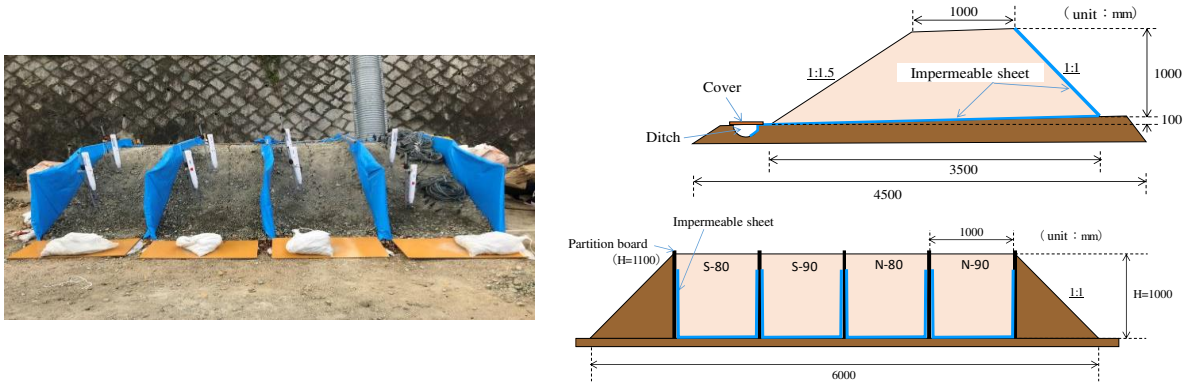

Figure 3. *Embankment model(Photo (left), Cross-section (upper right) and Front view (lower right))*

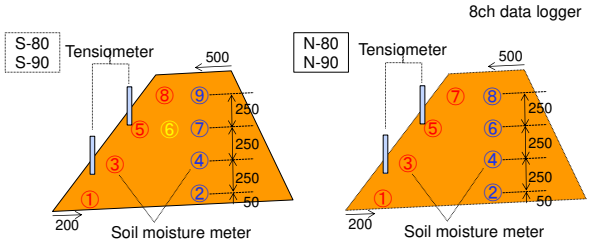

Figure 4. *Positions of monitoring meters*

3 EXPERIMENTAL RESULTS AND DISCUSSION

Figure 5 shows the precipitation and pH of leachate water during the monitoring term. The red and blue solid lines indicate the initial pH of the slag-mixed soil. Though the pH value during the dry term around at 50-100 days after construction dropped down once, it recovered during the rainy term at around 200 days.

These results indicate that the alkaline material contained in slag-mixed soil continues eluting to soil water until reaching equilibrium. Since the water content is high enough to dissolve alkaline material during the dry term, sporadic rainfall works to dilute the alkaline concentration of soil water. On the other hand, the amount of alkaline material eluted from slag-mixed soil was great within the high soil moisture embankment during the rainy term. Rainfall infiltration pushed this soil water containing alkaline material out of the embankment. Consequently, leachate behavior was different between the dry and the rainy terms.

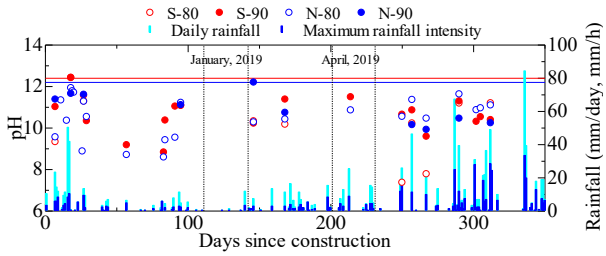

Figure 5. *Monitored pH of leachate water from the embankment*

Figure 6 shows soil moisture changes monitored at S-80 (Steel slag S mixed, 80% compaction degree). These data were monitored in January, with little rainfall, and in April, with periodic rainfall. Both 1ch and 2ch, positioned at the deepest area of the embankment, usually indicate high soil moisture, which facilitates the rise of the phreatic surface by infiltrated rainwater. Soil moisture around the slope surface (expressed by red lines) first increased when it rains. The increase in soil moisture of 2ch, positioned at

the center of the bottom of the embankment, was delayed in comparison with the other channels, as it took some time for infiltrated rainwater to reach the bottom. While soil moisture around the slope surface kept decreasing and reached equilibrium 3 days after the rain stops, it took more time for soil moisture at the center of the bottom to decrease. In fact, soil moisture increased gradually by the excess of infiltrated water over drainage under frequent rainfall. Previous work demonstrated through rainfall infiltration simulation on the slope model that the seepage behavior of rainwater differs between rainwater infiltrated through the slope surface and through the crown of the embankment (Kawai et al. 2017). The rainwater infiltrated through the crown flows vertically by elevation head difference and contributes to the rise of the phreatic surface after reaching the bottom. On the other hand, rainwater infiltrated through the slope surface tends to flow parallel to the slope surface, as unsaturated permeability around the slope surface increases. These behaviour can be seen in Figure 6. The soil moisture at 1, 3, 5 and 8ch installed close to the slope surface all shows clear increase due to rainfall. On the other hands, only soil moisture at the bottom shown in 2ch increases with a time lag after rainfall while the soil moisture at 4,7,and 9ch below the crown do not increase during rainfall. The infiltrated rainwater finally drains from the slope toe. Therefore, rainwater infiltrated through the slope surface has a higher hydraulic gradient than the one forming the phreatic surface and drains earlier.

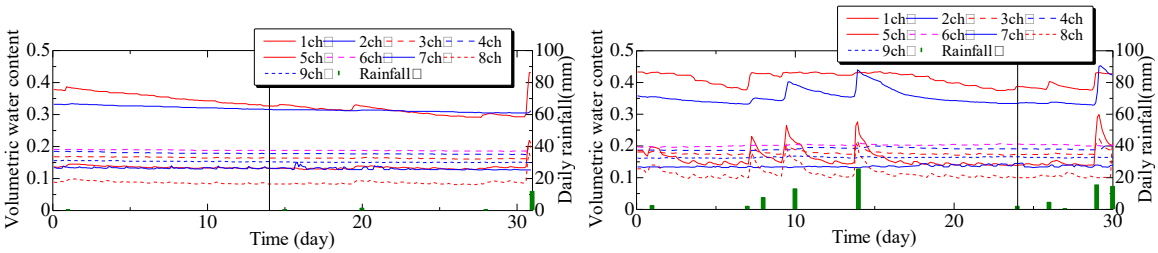

Figure 6. *Fluctuation in soil moisture (S-80) (January 2019 (left) and April 2019 (right))*

Figure 7 shows fluctuations in water pressure monitored by tensiometers over the same months. As indicated by the soil water retention characteristic curve, which expresses the relationship between suction (negative water pressure) and soil moisture, the sensitivity to rainwater differed between soil moisture and water pressure depending on the wetting condition. Suction (negative water pressure) increased even when it hardly rained and soil moisture hardly changed. This result underlines that it is important to monitor not only soil moisture but also suction for understanding seepage behavior.

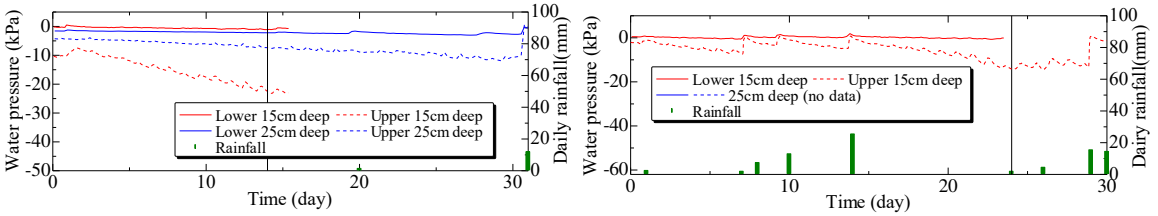

Figure 7. *Fluctuation in pore water pressure (S-80) (January 2019 (left) and April 2019 (right))*

Figure 8 shows electric resistibility distribution measured by the electrical prospecting on January 14th and April 24th. The dates of the electrical prospecting are expressed by the vertical solid line in Figures 6 and 7. The circled numbers, which indicate the position of soil moisture meters, are plotted in Figure 8 to compare with soil moisture monitored by the soil moisture meter. A redder area indicates higher electric resistibility and signifies lower soil moisture. Higher soil moisture appeared higher throughout the embankment in April, when it periodically rained, than in January, when it hardly rained. In both months, the steep slope side, which was covered with an impermeable sheet, shows low soil moisture and the toe of the more gradual slope, from where infiltrated rainwater drained, shows high soil moisture. Here, the result worthy of attention is that the area just below the slope shoulder shows low soil moisture. This tendency can be explained as follows. As detailed before, rainwater infiltrated through the slope surface tends to flow parallel to the slope surface, and rainwater infiltrated through the crown flows vertically; consequently, these two flows of rainwater avoid the area just below the slope shoulder. Additional water-sprinkle tests were conducted on the embankment model, namely S-80 and S-90, to investigate seepage behavior dependent on the surface through which rainwater infiltrates. Water was sprinkled with a hydraulic sprayer only on the crown of S-80 and only the upper two thirds of the gradual slope surface of S-90. Sprinkling time was controlled to achieve an infiltration of 5mm hourly and the sprinkling was conducted for a total of 7 times. The electrical prospecting was conducted 30 minutes

after each sprinkling. Figures 9 and 10 show the electric resistibility distribution measured by electrical prospecting before sprinkling and the condition after the 6th sprinkling, respectively. On embankment model S-80, for which water was only sprinkled on the crown, a low electric resistibility area appears only below the crown. On the other hand, on embankment S-90, both the sprinkled area of the upper two thirds of the slope surface and the slope toe indicate low electric resistibility. In order to understand these seepage behaviors theoretically and investigate the transport of alkaline components within the embankment, rainfall infiltration of embankment was simulated using soil/water/air/soluble material coupled analysis code, DACSAR-MPad (Nomura et al., 2018).

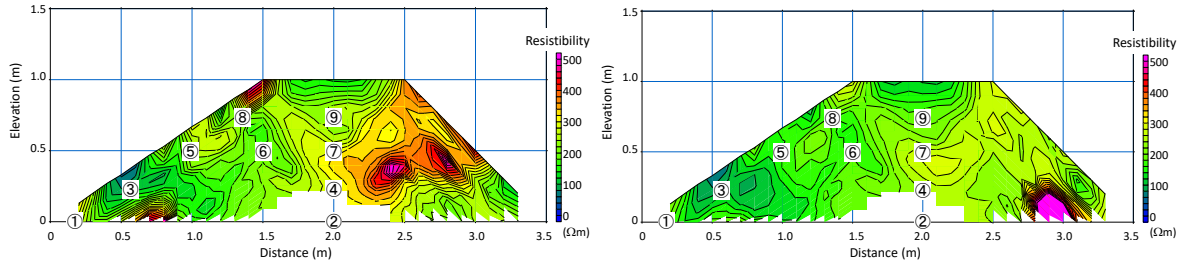

Figure 8. *Electric resistibility distribution (S-80) (January 14th, 2019 (left) and April 24th, 2019 (right))*

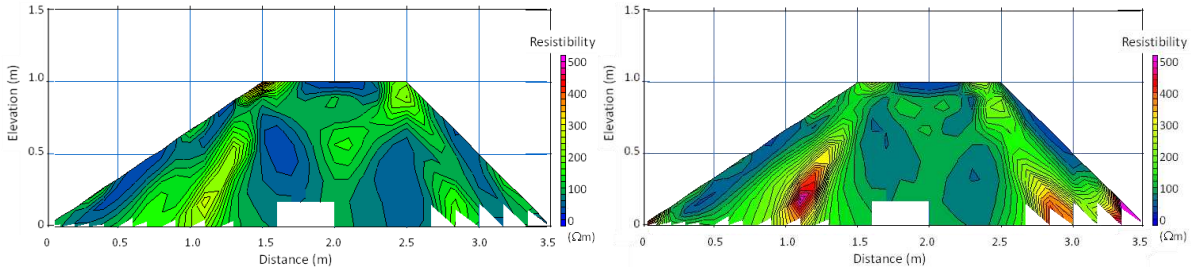

Figure 9. *Electric resistibility distribution before sprinkling (S-80 (left) and S-90 (right))*

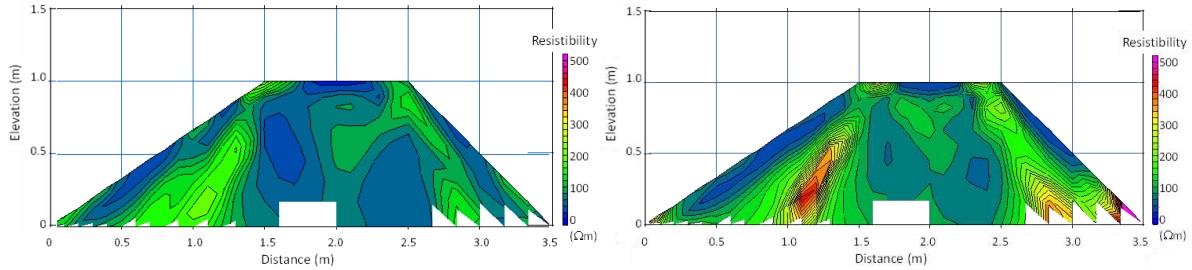

Figure 10. *Electric resistibility distribution after sprinkling 30mm (S-80 (left) and S-90 (right))*

4 MASS TRANSPORT INDUCED BY RAINFALL INFILTRATION IN SOIL/WATER/AIR/SOLUBLE MATERIAL COUPLED ANALYSIS

The analysis area model embankment test provided is shown in Figure 11. A non-permeable boundary was applied to the surface of the steeper slope and the bottom, and a water head boundary of -0.1 was applied to the slope toe. Rainfall was expressed as a flux boundary corresponding to rainfall intensity on the crown and the more gradual slope surface. Though in reality soluble material exits with leachate water, all boundaries were set as non-permeable in the material to clarify the localization of mass.

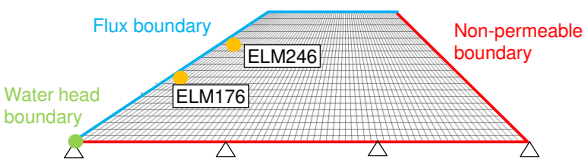

Figure 11. *Analytical mesh and boundary conditions*

Input parameters were determined based on experimental lab results and summarized in Table 2. Figure 12 shows the soil water retention characteristics.

Table 2. *Input material parameters*

λ	κ	M	m	n_E	a	n_s	γ	D_x	D_y
0.97	0.009	1.375	0.8	1.0	10.0	1.0	0.17	2.4×10^{-3}	2.4×10^{-3}

D_x , D_y :Dispersion coefficient, (m^2/day)

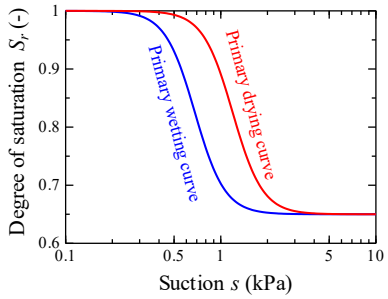

Figure 12. *Soil water retention characteristic curves used for simulation*

The optimum water content of 12%, suction of 1kPa, and relative concentration of 0.01 were applied to all elements first, and a settling period of 2 days was provided to create the simulation initial conditions shown in Figure 13. At these conditions, three kinds of rainfall patterns, 10mm/h×5h, 5mm/h×10h, and 2mm/h×25h, were applied to the crown and the more gradual slope surface. A settling period after rainfall was provided to investigate drainage behavior after the rainfall stopped.

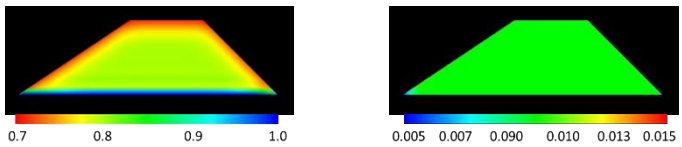

Figure 13. *Initial conditions (Degree of saturation (left) and Relative concentration (right))*

Figures 14 and 15 show the distribution in degree of saturation obtained from 10mm/h and 2mm/h rainfall simulations, respectively. As detailed before, it can be seen that there are two seepage behaviors, namely flow parallel to and around the slope surface and vertical flow below the crown. When the surface area of rainfall infiltration becomes saturated, rainwater cannot infiltrate anymore. This is called infiltration capacity. It takes a shorter time to reach infiltration capacity under a greater rainfall intensity. Therefore, a smaller rainfall intensity of 2mm/h, displays a greater amount of infiltrated rainwater under the same total precipitation. Consequently, a higher phreatic surface appears at smaller rainfall intensity after the rainfall stops.

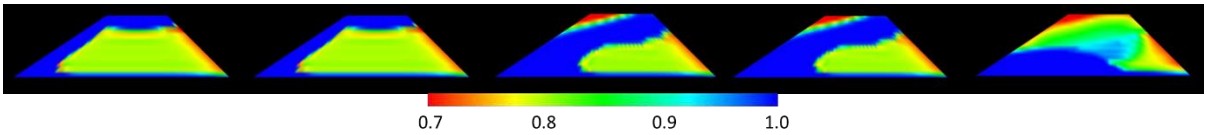

Figure 14. *Degree of saturation (10mm/h×5h) (from the left: 2.5h and 5h rainfall, 6h, 12h, and 24h after rain stops)*

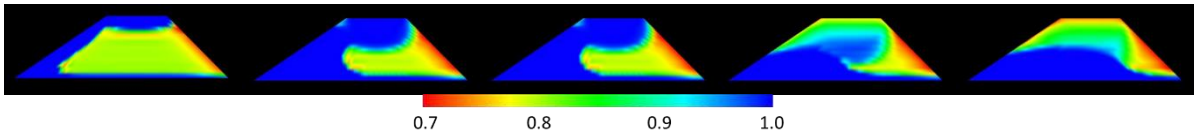

Figure 15. *Degree of saturation (2mm/h×25h) (from the left: 12.5h and 25h rainfall, 6h, 12h, and 24h after rain stops)*

Figures 16 and 17 show the distribution of relative concentration. Infiltrated rainwater finally drains from the more gradual slope toe, and a high relative concentration area appears at the slope toe. The flow

around the slope surface is relatively fast, and soluble material tends to be washed away. On the other hand, the vertical flow of rainwater infiltrated through the crown is slow and difficult to drain. The former tendency is more apparent under a larger rainfall intensity of 10mm/h, and the latter tendency is more apparent under a smaller rainfall intensity of 2mm/h. The elements 176 and 246 around the slope surface are focused to understand the accumulation of soluble material at the slope toe.

Figure 18 shows the fluctuation in the degree of saturation. In the figure, the time when rainfall stops is shown as dashed vertical lines. This figure shows that the elements reach infiltration capacity at all rainfall intensities, and saturation was reached earlier at higher rainfall intensity. Moreover, the lower element, 176, kept a higher degree of saturation even after rainfall stopped. This is because there was flow from the upper part of the slope.

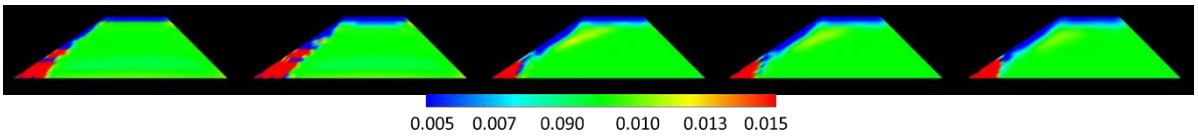

Figure 16. *Relative concentration (10mm/h×5h) (from the left: 2.5h and 5h rainfall, 6h, 12h, and 24h after rain stops)*

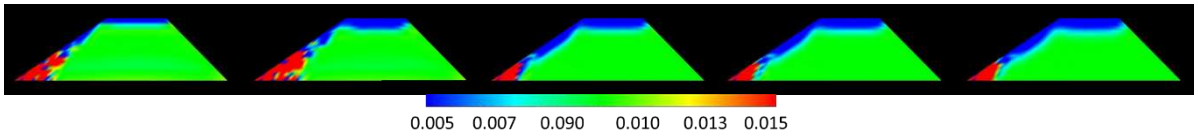

Figure 17. *Relative concentration (2mm/h×25h) (from the left: 12.5h and 25h rainfall, 6h, 12h, and 24h after rain stops)*

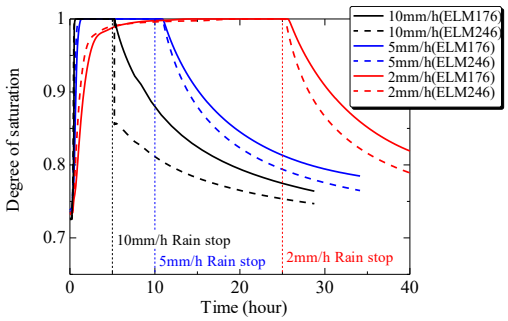

Figure 18. *Fluctuation in the degree of saturation at elements around the slope surface*

Figure 19 shows the fluctuation in relative concentration. Relative concentration decreases under rainfall, as soluble material is washed away. The tendency to recover relative concentration after rainfall stops is induced by dispersion of soluble material acculmulated at the slope toe. This results from the analysis condition, which does not permit soluble material to leach out of the embankment. Since in reality, soluble material leaches with drained rainwater from the embankment, the relative concentration would not increase again as shown in Figure 19. The way to apply a boundary condition that can express the transfer of soluble material within leachate water is left as an open question.

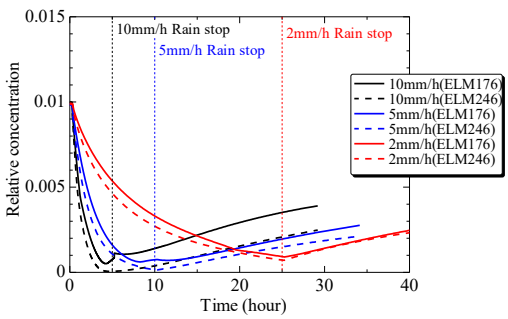

Figure 19. *Changes in relative concentration at elements around slope surface*

5 CONCLUSIONS

In this study, embankment model tests and rainfall infiltration simulations were conducted to investigate the transfer and leachate behavior of soluble material within an embankment constructed with steel slag-mixed soil. Two types of infiltrated rainwater flow were determined with their ratio dependent on rainfall intensity. This tendency influences soluble material transfer and dispersion. Numerical simulation can express seepage and leachate behaviour and is effective for designing embankment, such as its shape, the place of drainage, and so on, on mixture of soil and steel slag.

REFERENCES

Akinwumi, I. (2014). Soil modification by the application of steel slag. Periodica Polytechnica Civil Engineering, 58(4), 371-377.

Goodarzi, A. R. and Satimi, M. (2015). Stabilization treatment of a dispersive clayey soil using granulated blast furnace slag and basic oxygen furnace slag. Applied Clay Science, 108, 61-69.

Hirai, S., Mizutani, T., Kikuchi, Y. and Kawabata, Y. (2012). Study on effect of mixing condition on mechanical properties of mixture of dredged soil and steel slag. Report of the Port and Airport Research Institute, 51(3), 77-106 (in Japanese).

Kataoka, S., Shibuya, S. and Uematsu, S. (2017). Laboratory tests and a full-scale embankment of the mixture of slag and fine-grained soil. Proceedings of the 19th ICSMGE, 949-952.

Kawai, K., Kawakatsu, T. and Teraoka, A. (2017). Air pressure distribution induced by rainfall infiltration in soil/water/air coupled simulation. Internationa Journal of GEOMATE, 12(32), 63-69.

Malasavage, N. E., Jagupilla, S., Grubb, D. G., Wazne, M. and Coon, W. P. (2012). Geotechnical performance of dredged material-steel slag fines blends: laboratory and field evaluation. Journal of Geotehnical and Geoenvironmental Engineering, 138(8), 981-991.

Manso, J. M. Ortega-López, V., Polanco, J. A. and Setién, J. (2013). Tha use of ladle furnace slag in soil stabilization. Construction and Building Materials, 40, 126-134.

Nomura, S., Kawai, K., Tachibana, S. and Iizuka, A. (2018). Solute transfer during consolidation based on a solid-fluid-solute coupling model. International Journal for Numerical Analytical Methods in Geomechanics, 1-25.